ADVANCED MATERIALS
www.advmat.de

Monolayer Hexagonal Boron Nitride Films with Large Domain Size and Clean Interface for Enhancing the Mobility of Graphene-Based Field-Effect Transistors

Lifeng Wang, Bin Wu, Jisi Chen, Hongtao Liu, Pingan Hu, and Yunqi Liu**

A family of two dimensional (2D) materials has recently attracted intense interest due to their one-atom thickness and excellent physical properties in ambient conditions. The combination of these materials into stacked hybrid or in-plane heterogeneous structures may provide alternative functionality beyond pristine ones.[1] Hexagonal boron nitride (h-BN), a 2D insulator with a wide bandgap (5.97 eV), is structurally similar to graphene, consisting of alternating sp^2-bonded boron and nitrogen atoms in a plane with stacked layers held together by weak van der Waals forces.[2] h-BN has excellent physical properties such as high in-plane mechanical strength, high thermal conductivity, and high chemical stability,[3,4] and has proven to be a unique mate of graphene for improved device quality due to its atomically smooth surface that is relatively free of dangling bonds and charge traps.[5] The practical extension of this proof-of-concept is challenging, and requires greater control over scalable synthesis of h-BN film and related interfacial properties between these two materials during growth or post-growth process.

The chemical vapor deposition (CVD) method appears to be a promising method that allows the scaled synthesis of 2D materials and flexible manipulations of product properties such as grain size, layer number, crystallinity, and morphology. These features of this technique provide a practical route to overcome the drawbacks associated with the production of h-BN by the exfoliation method.[5] A few studies have been explored to grow h-BN films on certain substrates (Cu, Ni and Pt)[3,6–15] and the grown films were then incorporated into graphene device as a dielectric layer. While these studies demonstrated the possible solution for a few key issues such as the synthesis of continuous monolayer or thicker h-BN films, a wide landscape of the growth process was still not revealed and a better control of h-BN grain size for the production of high quality film has not realized. Moreover, the enhancement of the graphene carrier mobility has not been consistently achieved by using transferred as-grown h-BN film as a dielectric layer.[6,7] The possible reasons for this seemed to be complex, depending on many factors in the synthesis or transferring processes. These unresolved problems pointed to the importance of controlling h-BN quality and engineering the interfacial properties of h-BN film and graphene.

Here we report for the first time that using a system of h-BN growth on Cu surface under low-pressure CVD conditions, the nucleation density of h-BN can be significantly modulated in a large range, resulting in an effective control of h-BN grain sizes. These h-BN grains are single-layered, single crystals with a triangular shape, and the size can reach up to ca. 20 μm, 4–5 times larger than that in previously achieved results. We further discovered that h-BN grains can be directly visualized by optical microscopy by oxidizing Cu surface in air. Most importantly, it was found that interfacial properties of transferred h-BN films on SiO_2/Si substrate are critical to the device quality of stacked graphene material. We demonstrated that the contamination on h-BN film caused by the traditional poly(methyl methacrylate) (PMMA)-assisted transfer method is responsible for the degradation of graphene device quality, and the oxidation of h-BN film at high temperatures in air can effectively clean monolayer h-BN film interface, leading to reliable and much enhanced graphene mobility.

We used solid ammonia borane precursor to investigate the growth of h-BN on Cu surface under low pressure conditions. The precursor was heated by a separated heating belt, and the vapor of precursor molecules were introduced into the reaction zone by Ar carrier gas (see also the Materials and Methods section in the Supporting Information). As schematically shown in **Figure 1**a, within a range of temperatures (for example, 90–100 °C in our experiements), ammonia borane molecules dissociate into three products: hydrogen, polyiminoborane (BH_2NH_2; solid), and borazine ($(HBNH)_3$; gas).[9,10,13,16,17] Borazine molecules are the main building blocks for the growth of h-BN on the Cu surface at high growth temperatures. Experimentally, we found that the front side of Cu surface after growth was generally covered with a higher density of islands having white or black contrast as shown in Figure S1 in the Supporting Information. The formation of these objects was possibly related to precipitation of solid polyiminoborane byproducts on surface introduced by carrier gas or the existence of island growth mode except 2D grain expansion mode. However, the impurities can be dramatically reduced on the

L. F. Wang,[+] Dr. B. Wu,[+] J. S. Chen, H. T. Liu, Prof. Y. Q. Liu
Beijing National Laboratory for Molecular Sciences
Key Laboratory of Organic Solids
Institute of Chemistry
Chinese Academy of Science
Beijing, 100190, P. R. China
E-mail: liuyq@iccas.ac.cn
L. F. Wang, Prof. P. A. Hu
Key Lab of Microsystem and Microstructure
Harbin Institute of Technology
Harbin, 150080, P. R. China
E-mail: hupa@hit.edu.cn
[+]These authors contributed equally to this work

DOI: 10.1002/adma.201304937

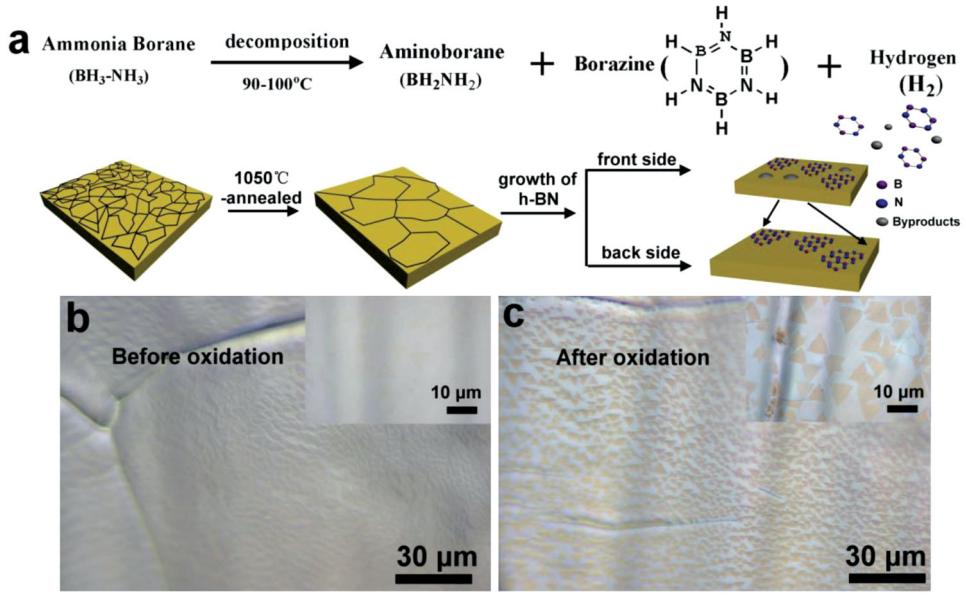

Figure 1. a) Upper schematic diagrams showing that ammonia borane dissociates into three products. Lower scheme of h-BN growth process showing the increased Cu grain sizes by thermal annealing and the different growth results of h-BN observed on the front and back-side of Cu foil. b,c) Optical images of h-BN domains grown on Cu surface with and without oxidation treatment in air, respectively. The inset in each image shows the corresponding close-up image.

back-side of Cu foil (See Figures 1b,1c and **Figure 2**), possibly due to the constrained diffusion of precursor molecules or by-products within the limited space in this case. In practice, this finding is important for clean h-BN synthesis, and it also establishes a standard on which all the following investigations of h-BN growth are based.

The product with the best well-defined geometric structure on Cu surface was synthesized by using pure Ar carrier gas with a flow rate of about 40 sccm (standard cubic centimeters per minute) at the growth temperature of 1000 °C and a pressure of about 30–40 Pa. Figure 1b shows a typical optical image of a sample after growth in which there are no clear features indicating the existence of h-BN. As any change of light reflection behavior of two materials on surface could make them visible in optical microscopy, we simply oxidized the sample in air at 100 °C for 1 h. This treatment resulted in an oxidation of Cu surface, making the contrast of h-BN with respect to adjacent Cu surface appear as shown in Figure 1c. Although this technique was previously used for direct visualization of graphene domains on Cu surface,[18] it was the first application to h-BN flakes on Cu

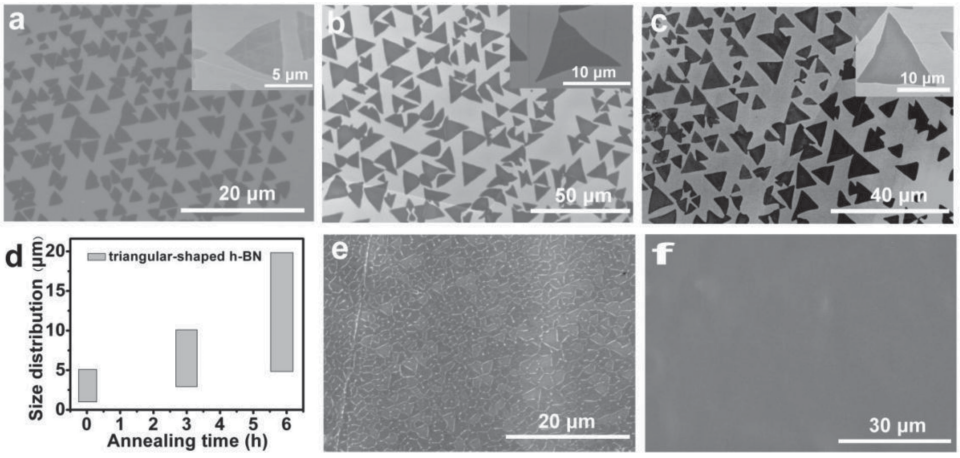

Figure 2. a) SEM image of triangular-shaped h-BN domains grown on Cu foil surface without pre-annealing. b,c) SEM images of h-BN domains grown on annealed Cu surface for 3 h and 6 h, respectively. The rest growth conditions for (a)–(c) are the same: using 40 sccm Ar at the pressure of 30–40 Pa at 1000 °C for 60 min. d) A graph showing the size distributions of h-BN domains as a function of annealing time for Cu foils. e,f) SEM images showing that h-BN domains grow into near-fully covered and continuous film for a longer growth time of 65 min and 70 min, respectively.

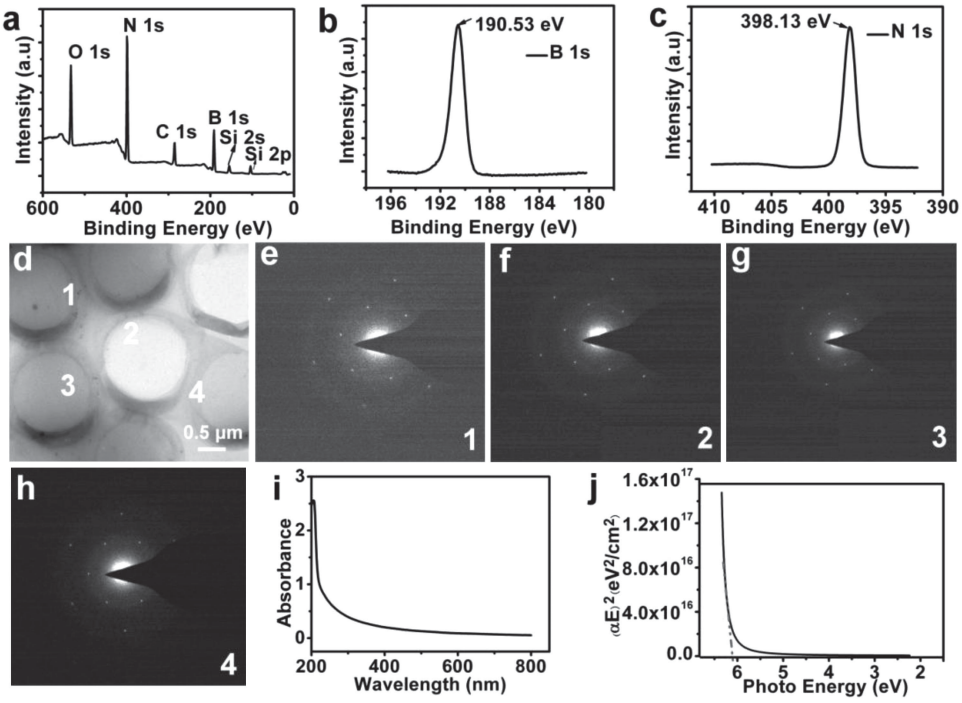

Figure 3. a) XPS survey spectrum of transferred h-BN films on SiO_2/Si substrates, where Si and O peaks are from substrates. b,c) The corresponding XPS spectra of B 1s and N 1s, respectively. d) A typical TEM image of a continuous h-BN film on holey carbon grid. e–h) SAED patterns recorded on different locations labeled in image (d). i) UV–vis spectrum of a monolayer h-BN film on transparent quartz substrate. j) OBG calculation plot of h-BN film.

surface. Triangular-shaped h-BN flakes can be clearly identified as darker region in the optical image of Figure 1c, and this well-defined shape is an indication of single-crystal h-BN domains as observed in previous work.[10,12,14,15] Note that graphene domains on Cu surface show the brighter contrast with respect to adjacent oxidized Cu surface.[19]

Continuous film grown by nucleation and growth mechanism is polycrystalline, composed of interconnected grains. In general, large-sized grains produce a low density of grain boundaries per area in the film, resulting in a higher quality of film for electronic device applications. We found that it was possible to effectively manipulate the nucleation process in a controlled manner. As the nucleation generally occurs on higher surface energy regions such as grain boundaries or impurity sites, it would be expected to tune nucleation density by engineering Cu surface crystallinity. Along this line, Cu foils were annealed under Ar/H_2 atmosphere at 1050 °C for 3 and 6 h for comparison. Thermal annealing of Cu foils led to an increase of its grain size and an improved surface flatness by eliminating grain boundaries or defects (Figure S2a and S2b, Supporting Information). Figures 2a,2b and 2c show scanning electron microscopy (SEM) images of triangular-shaped h-BN flakes formed on Cu foils using the same growth conditions with different thermal annealing times. These images clearly showed that the size distributions of h-BN flakes changed approximately from 1–5 to 3–10 to 5–20 μm for annealing time of 0, 3 and 6 h, respectively. Figure 2d shows the corresponding distributions of h-BN size obtained from many SEM images for three cases. The size of these h-BN flakes was 4–5 times larger than the size of 1–5 μm achieved in previous studies.[10,14,15] The analyzed nucleus density in each case shown in Figure S3 in the Supporting Information exhibited a monotonical decrease with increasing annealing time of Cu foils. Note that the estimated growth rates for each case essentially remained the same (about 0.5–1 μm/min obtained by comparing the different average sizes at different growth time). These results indicate that the formation of large sized h-BN domains is mainly attributed to reduced nucleation density for annealled Cu surface. The value of growth rate actually is a kind of intrinsic properties reflecting the interplay of many microscopic processes at the special condition, and it is useful for predicting the growth time for specific size of h-BN flakes. Further increasing the growth time led to a decreased gap (the white lines in Figure 2e) among the h-BN flakes, and these flakes were eventually connected to form a continuous film with a uniform appearance as shown in Figure 2f.

X-ray photoemission spectroscopy (XPS) was performed on transferred h-BN films (see the Materials and Methods section in the Supporting Information) on 300 nm SiO_2/Si substrates to determine the chemical composition of the product as shown in **Figure 3**a–c. The observed binding energies of N 1s and B 1s are 398.13 and 190.53 eV, respectively. The values are in good agreement with the literature values.[3,9–13] The B/N ratio from our XPS survey was calculated to be 1.07. Both the B 1s and the N 1s spectra indicate that the configuration for B and N atoms is the B-N bond, implying that the hexagonal phase exists in our BN films.

Transmission electron microscopy (TEM) was used to characterize the crystalline structure of grown h-BN film. Note that individual h-BN flakes are difficult to be identified in TEM due

to very low contrast. Figures 3d– 3h show a TEM image of h-BN film transferred onto TEM grid together with selected area electron diffraction (SAED) patterns recorded at different locations. The profile of film appears homogeneous in Figure 3d, and the corresponding SAED patterns show the characteristic 6-fold symmetric diffraction spot of h-BN materials, indicating well-crystalline structure of as-grown sample. Note that only one set of diffraction patterns was observed, strongly indicating that as-grown h-BN was single-layered. Moreover, diffraction patterns recorded at random selected different locations in the film always show the same orientated SAED patterns within an area (Figures 3e–3g), and the SAED pattern for locations farther away from the area exhibits the different orientation as shown in Figure 3h, demonstrating that the continuous film is composed of single-crystalline building blocks with different orientation. The results are consistent with SEM observations that triangular-shaped h-BN grains grow into the continuous film with an extended growth time.

To further confirm the existence and quality of monolayer h-BN films, they were transferred onto transparent quartz substrates, and then analyzed by the optical absorption technique. Figure 3i shows a UV–visible absorption spectrum of single-layer h-BN. h-BN film exhibits almost zero absorbance in the visible-light range and an abrupt absorption in the UV region. This indicates the presence of an optical bandgap (OBG). By using the formula for a direct band semiconductor,[20] OBG is determined to be 6.07 eV as shown in Figure 3j (see the Materials and Methods section in the Supporting Information).[12,20] This value is slightly larger than that of bulk h-BN or few layer h-BN, which can be attributed to the fact that there is no layer–layer interaction in monolayer h-BN.[21] In fact, this value is consistent with that for monolayer h-BN predicted by theoretical calculations (6.0 eV)[22] and determined by previous experiments.[10,13]

Detailed studies have been further performed to better understand h-BN growth process. We have systematically studied the effect of various experimental conditions such as growth temperature, precursor temperature, growth time and the pressure of reaction chamber on grown product. For example, we found that growth temperature had a profound impact on the final product. There were four regions of growth identified. At 450–650 °C, Cu surface became rough, and there existed particle-like products on surface, but no sign of sheet-like products formed (Figures S4a–4c, Supporting Information). Note that the dehydrogenation temperature of the poly(borazylene) film is above 700 °C.[6] These results indicate that the dehydrogenation is a necessary step for the formation of h-BN nuclei and growth. At 750–970 °C, irregular shaped feature with dark contrast in Figures S4d–4g can be clearly observed. Further increasing growth temperature to 1000 °C led to a dramatic change of feature's geometric shape: well-defined triangular-shaped h-BN flakes are formed on Cu surface (Figure S4h, Supporting Information). However, these shaped features disappeared when higher growth temperature was applied (Figure S4i, Supporting Information). Note that growth temperature also affects the nucleation density as shown in Figure S5 in the Supportign Information, that is to say, the higher the temperature is, the larger the average h-BN grain size is. This trend is generally valid from the thermodynamical point of view, and is consistent with the behavior observed in the case of graphene growth.[19] It is expected that much larger-sized grains could be grown by using these principles to further engineer the related experimental conditions.

The growth is also sensitive to the chamber pressure. Figure S6 in the Supporting Information shows that the morphologies of the product are different under different chamber pressures (30–40 Pa, 130 Pa and 230 Pa), respectively. In contrast, we did not find a large effect on the growth with precursor temperatures in the range of 90–100 °C. Although these systematic investigations of the growth process provide rich phenomenal evidences of this complex growth system, the microscopic mechanism regarding the correlation between various experimental parameters and the corresponding product still needs to be addressed in future work.

The thickness of triangular-shaped h-BN layer transferred onto a SiO_2/Si substrate can be determined using atomic force microscopy (AFM). **Figure 4**a shows the AFM image of triangular-shaped h-BN flakes on a SiO_2/Si substrate. The whole surface is covered with PMMA residues due to transferring process, and the typical thickness of h-BN flake is 1.82–1.99 nm. Due to the super oxidation stability of h-BN at high temperature in air, transferred triangular-shaped h-BN flakes were annealed at 950 °C in air for 20 min to remove PMMA residues. After this treatment, the residues of PMMA on surface were almost completely removed as confirmed by AFM image in Figure 4b. Clean h-BN flakes give a height value of about 0.59 nm and a surface roughness of 0.13 nm (Figure 4b inset), and these values are well consistent with those for single-layer h-BN.[10,13] Figure S7 in the Supporting Information shows optical images of continuous h-BN films transferred on SiO_2/Si substrate after the treatment, confirming that the treatment can effectively clean h-BN surface without the damage of h-BN film continuity.

We fabricated field-effect transistor (FET) devices of monolayer hexagnoal graphene flakes grown on liquid Cu surface[23,24] using untreated and oxidation-cleaned h-BN monolayer film as dielectrics. Briefly, monolayer h-BN films were transferred onto 300 nm SiO_2/Si substrate, followed by transferring graphene flakes onto h-BN films with or without oxidation treatment. Device fabrication procedures were similar to that previously reported,[23,24] and electrical transport measurements were conducted in amibent condition. Figure 4c shows a typical optical image of graphene/h-BN film FET device. More than 20 devices were tested to compare the difference of two type samples in electrical properties. In all cases, using clean h-BN films as dielectrics exhibits the improvement of graphene carrier mobility and the downshift of Dirac point compared to using untreated h-BN film. Figure 4d shows representive transfer curves for two cases. The devices of two type of samples show p-type behavior similar to our previous results for graphene sample on SiO_2/Si substrate.[24] The shifting of Dirac points for two cases can be clearly seen, with V_g = 65 V for untreated h-BN film (upper curve) and V_g = 58 V for treated sample. This trend is still valid by including the case of graphene on SiO_2/Si substrate as its Dirac point cannot be observed in most cases using a similar device fabrication procedure and device measurements.[24]

The shifting of the Dirac points for graphene devices is an indicator of graphene doping by substrates or environment.

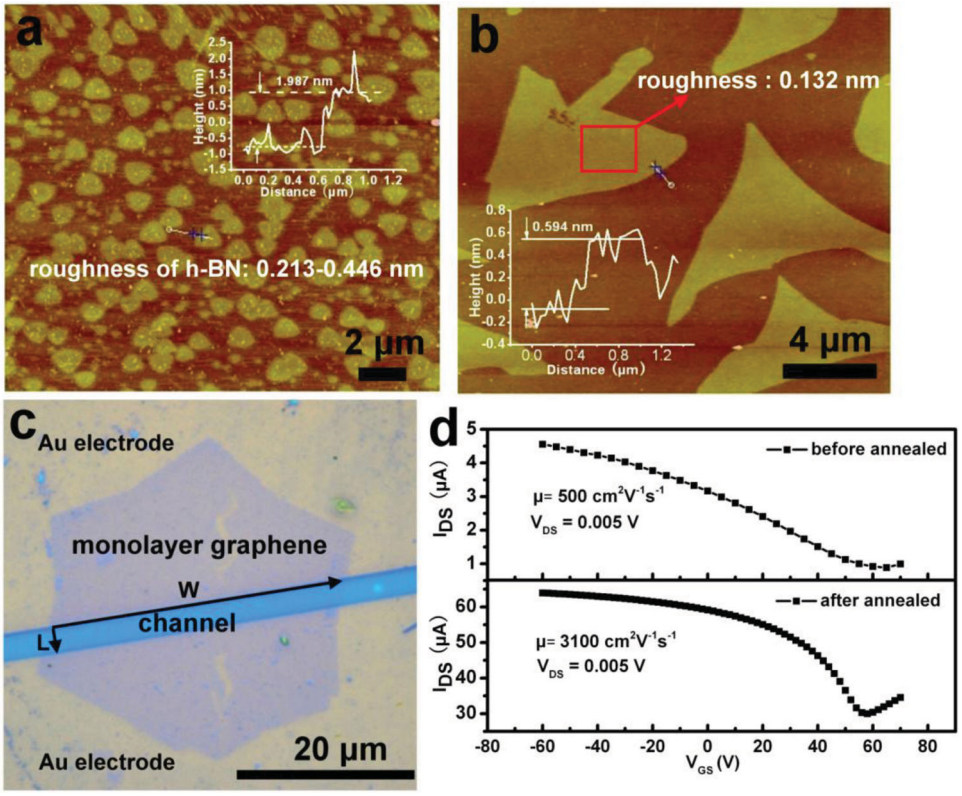

Figure 4. a,b) Typical AFM images of h-BN grains transferred onto SiO_2/Si substrates by the PMMA-assisted method before and after oxidation treatment, respectively. Insets in each image also show the height of h-BN grain along the labeled lines and roughness value measured on h-BN surface. c) Optical image of one typical graphene/h-BN film FET device showing hexagonal graphene flake and top/bottom Au electrodes. Channel length and width are also indicated in image. d) Transfer curves of graphene/h-BN films before (upper curve) and after (lower curve) the removal of PMMA residues by oxidation (labeled as before and after annealed in plots) in air at high temperatures, respectively. Note that the values of hole mobility are indicated in insets.

Specifically, the relative shifting of Dirac points can be attributed to different p-doping level of graphene by trapped charges on surfaces of substrates, among which clean h-BN surface has the mimimum density of trapped charges. Excluded from the substrate doping effect, the Dirac point at high V_g associated with graphene doping is likely to be related to the presence of oxygen, water adsorbents from the environment or PMMA residues left on the graphene surface during the transfer process. A typical Raman spectrum of transferred graphene on SiO_2/Si substrate shown in Figure S8 in the Supporting Information exhibits graphene doping features. For example, the G and 2D bands are located in the range of 1585–1595 and 2685–2695 cm^{-1} with an intensity ratio (2–3) of the 2D to the G band, respectively. These features indicate a p-doping of transferred graphene.[25] In addition, device fabrication procedures such as the type of metal electrodes and thermal annealing process may also change the apparent location of Dirac points. We used the same device fabrication procedures to compare the roles of substrates for graphene device performance. These results demonstrate the important role of interfacial properties between substrate and graphene in determining graphene device performance. Indeed, graphene devices on cleaned h-BN films show much enhanced hole carrier mobility. For example, the calculated hole carrier mobility is about 3100 $cm^2\ V^{-1}\ s^{-1}$ at V_{ds} = 0.005 V, which is about 6-fold higher than the value of 500 $cm^2\ V^{-1}\ s^{-1}$ at V_{ds} = 0.005 V in the case of graphene on untreated h-BN monolayer.

In summary, we have demonstrated an effective means to tune the size of single-crystalline h-BN flakes by thermally annealing Cu foils. A facile technique was used to optically visualize the individual h-BN grains. By considering the super oxidation stability of h-BN at high temperature, we demonstrated that PMMA residues can be effectively removed without damage of monolayer h-BN film. This clean interface between h-BN film and transferred graphene flake is critical for achieving the reliable and improved device quality of graphene.

Experimental Section

The h-BN flakes were produced on Cu surface using the ammonia borane CVD method at various conditions (see also the Materials and Methods section in the Supporting Information). The samples were characterized by optical microscopy, scanning electron microscopy (SEM) (Hitachi S-4800, 1 kV and 15 kV), UV–vis absorption spectroscopy, atomic force microscopy (AFM) (Vecco Nanoman VS in the tapping mode) and transmission electron microscopy (Tecnai G2 F20 U-TWIN, operated at 200 kV). Individual graphene flakes contacted with source and drain

electrodes on h-BN/SiO_2/Si substrate were fabricated as FET devices, and the electrical characterization was tested using a Keithley 4200 instrument at room temperature in air (see also the Materials and Methods section in the Supporting Information).

Supporting Information

Supporting Information is available from the Wiley Online Library or from the author.

Acknowledgements

The authors gratefully acknowledge financial support from the National Basic Research Program of China (2011CB932700, 2011CB932303, 2011CB808403, 2013CB933500), the National Natural Science Foundation of China (61171054, 21273243, 20973184, 60911130231), and the Chinese Academy of Sciences.

Received: October 3, 2013
Revised: October 28, 2013
Published online: December 17, 2013

[1] A. K. Geim, I. V. Grigorieva, *Nature* **2013**, *499*, 419–425.
[2] K. Watanabe, T. Taniguchi, H. Kanda, *Nat. Mater.* **2004**, *3*, 404–409.
[3] L. Song, L. Ci, H. Lu, P. B. Sorokin, C. H. Jin, J. Ni, A. G. Kvashnin, D. G. Kvashnin, J. Lou, B. I. Yakobson, P. M. Ajayan, *Nano Lett.* **2010**, *10*, 3209–3215.
[4] Y. Chen, J. Zou, S. J. Campbell, G. Le Caer, *Appl. Phys. Lett.* **2004**, *84*, 2430–2432.
[5] C. R. Dean, A. F. Young, I. Meric, C. Lee, L. Wang, S. Sorgenfrei, K. Watanabe, T. Taniguchi, P. Kim, K. L. Shepard, J. Hone, *Nat. Nanotechnol.* **2010**, *5*, 722–726.
[6] K. K. Kim, A. Hsu, X. T. Jia, S. M. Kim, Y. M. Shi, M. Dresselhaus, T. Palacios, J. Kong, *ACS Nano* **2012**, *6*, 8583–8590.
[7] K. H. Lee, H. J. Shin, J. Lee, I. Lee, G. H. Kim, J. Y. Choi, S. W. Kim, *Nano Lett.* **2012**, *12*, 714–718.
[8] M. Wang, S. K. Jang, W. J. Jang, M. Kim, S. Y. Park, S. W. Kim, S. J. Kahng, J. Y. Choi, R. S. Ruoff, Y. J. Song, S. Lee, *Adv. Mater.* **2013**, *25*, 2746–2752.
[9] Y. M. Shi, C. Hamsen, X. T. Jia, K. K. Kim, A. Reina, M. Hofmann, A. L. Hsu, K. Zhang, H. N. Li, Z. Y. Juang, M. S. Dresselhaus, L. J. Li, J. Kong, *Nano Lett.* **2010**, *10*, 4134–4139.
[10] K. K. Kim, A. Hsu, X. T. Jia, S. M. Kim, Y. M. Shi, M. Hofmann, D. Nezich, F. Joaquin, M. Dresselhaus, T. Palacios, J. Kong, *Nano Lett.* **2012**, *12*, 161–166.
[11] G. Kim, A.-R. Jang, H. Y. Jeong, Z. Lee, D. J. Kang, H. S. Shin, *Nano Lett.* **2013**, *13*, 1834–1839.
[12] W. Auwärter, H. U. Suter, H. Sachdev, T. Greber, *Chem. Mater.* **2004**, *16*, 343–345.
[13] Y. Gao, W. C. Ren, T. Ma, Z. B. Liu, Y. Zhang, W. B. Liu, L. P. Ma, X. L. Ma, H. M. Cheng, *ACS Nano* **2013**, *7*, 5199–5206.
[14] A. Ismach, H. Chou, D. A. Ferrer, Y. P. Wu, S. McDonnell, H. C. Floresca, A. Covacevich, C. Pope, R. Piner, M. J. Kim, R. M. Wallace, L. Colombo, R. S. Ruoff, *ACS Nano* **2012**, *6*, 6378–6385.
[15] S. M. Kim, A. Hsu, P. T. Araujo, Y. Lee, T. Palacios, M. Dresselhaus, J. Idrobo, K. K. Kim, J. Kong, *Nano Lett.* **2013**, *13*, 933–941.
[16] F. Baitalow, J. Baumann, G. Wolf, K. Jaenicke-Robler, G. Leitner, *Thermochemical. Acta* **2002**, *391*, 159–168.
[17] S. Frueh, R. Kellett, C. Mallery, T. Molter, W. S. Willis, C. King'ondu, S. L. Suib, *Inorg. Chem.* **2011**, *50*, 783–792.
[18] H. Wang, G. Z. Wang, P. F. Bao, S. L. Yang, W. Zhu, X. Xie, W. J. Zhang, *J. Am. Chem. Soc.* **2012**, *134*, 3627–3630.
[19] B. Wu, D. C. Geng, Y. L. Guo, L. P. Huang, Y. Z. Xue, J. Zheng, J. Y. Chen, G. Yu, Y. Q. Liu, L. Jiang, W. P. Hu, *Adv. Mater.* **2011**, *23*, 3522–3525.
[20] T. H. Yuzuriha, D. W. Hess, *Thin Solid Films* **1986**, *140*, 199–207.
[21] D. M. Hoffman, G. L. Doll, P. C. Eklund, *Phys. Rev. B* **1984**, *30*, 6051.
[22] X. Blasé, A. Rubio, S. G. Louie, M. L. Cohen, *Phys. Rev. B* **1995**, *51*, 6868–6875.
[23] D. C. Geng, B. Wu, Y. L. Guo, L. P. Huang, Y. Z. Xue, J. Y. Chen, G. Yu, L. Jiang, W. P. Hu, Y. Q. Liu, *Proc. Natl. Acad. Sci. USA* **2012**, *109*, 7992–7996.
[24] B. Wu, D. C. Geng, Z. P. Xu, Y. L. Guo, L. P. Huang, Y. Z. Xue, J. Y. Chen, G. Yu, Y. Q. Liu, *NPG Asia Mater.* **2013**, *5*, e36.
[25] A. Das, S. Pisana, B. Chakraborty, S. Piscanec, S. K. Saha, U. V. Waghmare, K. S. Novoselov, H. R. Krishnamurthy, A. K. Geim, A. C. Ferrari, A. K. Sood, *Nat. Nanotechnol.* **2008**, *3*, 210–215.